



Interaction-driven topological phase transition in monolayer $\text{CrCl}_2(\text{pyrazine})_2$ Xuecong Ji ^{1,2,*} Jiacheng Gao,^{1,2,*} Changming Yue ³ Zhijun Wang ^{1,2} Hua Wu,^{4,5}
Xi Dai,^{6,†} and Hongming Weng ^{1,2,7,‡}¹*Beijing National Laboratory for Condensed Matter Physics,
and Institute of Physics, Chinese Academy of Sciences, Beijing 100190, China*²*University of Chinese Academy of Sciences, Beijing 100049, China*³*Department of Physics, University of Fribourg, 1700 Fribourg, Switzerland*⁴*Laboratory for Computational Physical Sciences (MOE), State Key Laboratory of Surface Physics,
and Department of Physics, Fudan University, Shanghai 200433, China*⁵*Collaborative Innovation Center of Advanced Microstructures, Nanjing 210093, China*⁶*Department of Physics, Hong Kong University of Science and Technology, Kowloon 999077, Hong Kong, China*⁷*Songshan Lake Materials Laboratory, Dongguan, Guangdong 523808, China*

(Received 16 August 2022; accepted 21 November 2022; published 5 December 2022)

The quadratic band crossing points (QBCPs) at the Fermi level in two dimensions have been proposed to be unstable under electron-electron interactions. The possible interaction-driven states include the quantum anomalous Hall (QAH) state and various nematic ordered states. In this paper, motivated by the discovery of ferromagnetic van der Waals layered metal-organic framework $\text{CrCl}_2(\text{pyrazine})_2$, we theoretically propose that a single layer of $\text{CrCl}_2(\text{pyrazine})_2$ might realize one or some of these interaction-driven states based on the QBCP protected by C_4 symmetry. By introducing short-range density-density type repulsion interactions into this system, we have found the phase diagram depending on different interaction ranges and strengths. The exotic phases include the staggered chiral flux state manifesting the QAH effect, the site-nematic insulator, and the site-nematic Dirac semimetal state. The QAH state is robust against perturbations breaking the QBCP but it is weakened by increasing temperature. The metal-organic framework is tunable by changing the transition-metal elements, which might improve the gap size and stability of this interaction-induced QAH state.

DOI: [10.1103/PhysRevB.106.235103](https://doi.org/10.1103/PhysRevB.106.235103)**I. INTRODUCTION**

In the past decades, quantum anomalous Hall (QAH) states have aroused great interests in the condensed matter physics community [1–8]. Different from the quantum Hall effect, the chiral edge state of a QAH insulator results from the breaking of time-reversal symmetry (TRS) without introducing an external magnetic field. Recently, the QAH effect has been realized in magnetically doped [3,7,9] or intrinsic two-dimensional ferromagnetic topological insulators [10–12] at extremely low temperatures. The improvement of critical temperature is highly needed for extensive studies and potential applications, but it is quite challenging. One of the reasons is that in these realizations the bulk gap is opened and limited by the effective strength of the spin-orbit coupling (SOC) of the inverted valence and conduction bands, which leads to a nonzero Chern number.

This band gap limitation might be avoided in the interaction-induced QAH insulator state proposed in various schemes [13–22]. Especially, the quadratic band crossing point (QBCP) in two-dimensional systems is proved to be unstable against arbitrarily weak short-range repulsive

interactions [18–24]. The resulting gapped phases are QAH or nematic state depending on the interaction parameters and temperature. The QBCP semimetal state requires the protection of fourfold or sixfold rotational symmetry [18,19]. In the typical checkerboard lattice model satisfying C_4 rotation symmetry, a fairly large next-nearest-neighbor (NNN) hopping parameter is assumed. Otherwise, the QAH phase would be dominated by the nematic phase even in low temperature, or the QAH order parameters are too small to be observed [18,19].

Recently, the ferromagnetic van der Waals layered metal-organic framework $\text{CrCl}_2(\text{pyz})_2$ (where pyz stands for pyrazine) has been synthesized and the Curie temperature is found to be 55 K [25]. First-principles calculations [26,27] and experimental measurements [25,28] all confirm its ferromagnetic ground state. While first-principles calculations give a semimetallic band structure [26,27], the conductivity measurement [25] suggests an insulating ground state. In this paper, we proposed $\text{CrCl}_2(\text{pyz})_2$ to be the material realizing a two-dimensional spinless QBCP model on a checkerboard lattice. To achieve the insulating ground state, short-range Coulomb interactions have been taken into consideration under the mean-field level. In this realistic system, the amplitude of NNN hopping is fairly small compared to the nearest-neighbor (NN) hopping. To explore more possible phases in this system, we added two types of NNN interactions that have been considered based on the crystal structure of

*These authors contributed equally to this work.

†daix@ust.hk

‡hmweng@iphy.ac.cn

$\text{CrCl}_2(\text{pyz})_2$. The QAH state appears in the phase diagram when the strength of the NNN interaction is close to the NN hopping amplitude. In addition, we found another type of nematic phase with Dirac points. Furthermore, we find the site-nematic Dirac semimetal state is also possible.

II. FIRST-PRINCIPLES CALCULATIONS

The first-principles calculations are based on density functional theory (DFT) [29] using the Vienna *ab initio* simulation package (VASP) [30]. The wave function is expressed with the plane-wave basis set and the exchange and correlation effect are described by the generalized gradient approximation (GGA) with the Perdew-Burke-Ernzerhof (PBE) functional [31,32]. The kinetic energy cutoff for the plane-wave basis is set to 500 eV. In the self-consistent calculation, a Monkhorst-Pack [33] k mesh of $9 \times 9 \times 1$ is used for the Brillouin zone integration. We use the GGA+ U method [34] with Hubbard $U = 4.0$ eV and Hund exchange $J = 0.9$ eV for the $3d$ orbitals of Cr [26].

The monolayer $\text{CrCl}_2(\text{pyz})_2$ is crystallized in space group $P4/nbm$ [27] with the fourfold rotation axis perpendicular to the layer and passing through Cr atoms. There are four pyrazine rings in each primitive cell as shown in Fig. 1(a). The arrows are the in-plane projections of the normal vectors of pyrazine rings. They are along the diagonal lines of the cell. Within the GGA+ U first-principles calculation, the ferromagnetic order on Cr gives out a semimetal-type band structure, as shown in Fig. 1(b). The four bands around the Fermi level are dominantly contributed by the spin-down p orbitals from the C and N atoms on the pyrazine rings, separating from the spin-up conducting bands. The gap between spin-up bands and spin-down bands does not change with the on-site Hubbard U but the bandwidth of the spin-down bands around the Fermi level is slightly decreased by increasing the value of U . The SOC effect is fairly weak because these bands are coming from the $2p$ orbitals of C and N atoms and they are strongly spin polarized. The polarization of pyrazine rings is opposite to Cr ions and it is also looked at as a ferrimagnetic state [25].

The QBCP at the Γ point is protected by \tilde{C}_4 symmetry ($\tilde{C}_4 = \{C_4|1/2, 0, 0\}$). A slight breaking of \tilde{C}_4 but preserving \tilde{C}_2 would split the QBCP into two Dirac points with a linear dispersion [19]. The parities of the Bloch states on the time-reversal invariant momenta (TRIM) around the Fermi level are labeled in Fig. 1(b), from which we can deduce that a gapped state of the system without further band inversion at M would lead to a QAH state. From the topological quantum chemistry analysis [35–37], these four bands come from the elementary band representation (EBR) $A_u @ 4f$. The Wyckoff position $4f$ exactly sits at the center of four pyrazine rings, which indicates the low-energy bands come from the effective molecular orbitals of pyrazine rings. The site symmetry group of the ring center is $2/m$, in which the twofold rotational axis is along the diagonal axis of the primitive cell. Thus, the A_u representation on each site is embedded by any p orbital perpendicular to this in-plane C_2 rotation axis. For such a reason, we choose the p orbitals parallel to the arrows in Fig. 1(a) to construct the effective model Hamiltonian.

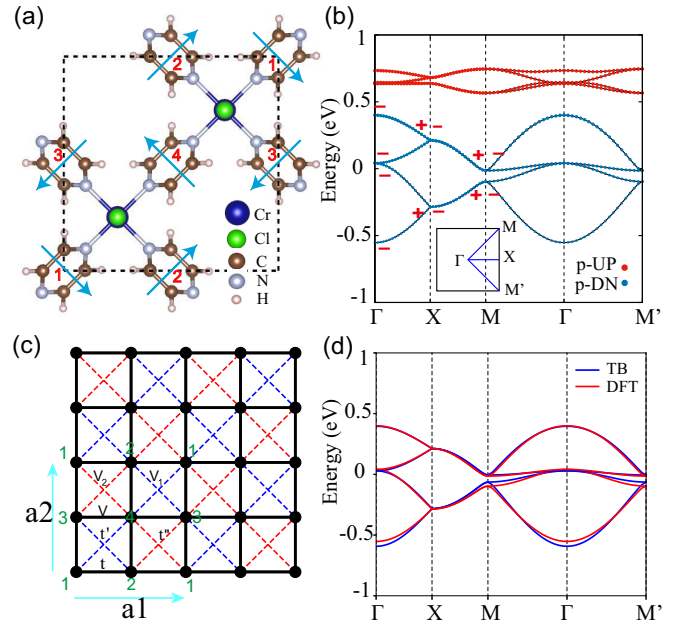


FIG. 1. (a) The top view of monolayer $\text{CrCl}_2(\text{pyz})_2$. The arrows represent the in-plane projection of pyrazine rings' normal vectors. We label the four rings from 1 to 4. (b) The DFT band structure of ferromagnetic $\text{CrCl}_2(\text{pyz})_2$. The red and blue dots represent the spin-up and spin-down p -orbital weight from the C and N atoms. On each TRIM, the parities of the four states around the Fermi level are labeled with + and - for even and odd, respectively. The inset is the Brillouin zone (BZ) and high-symmetry points. (c) The graphic plot of the low-energy effective model. The black solid lines represent the hopping amplitude t and interaction strength V among NN sites. The blue dashed lines represent NNN hopping t' and interaction V_1 with Cr atoms as the intermediate site, while the red dashed lines represent t'' and V_2 without intermediating Cr. (d) The fitted band structure of the four bands near the Fermi level with an effective tight-binding Hamiltonian.

III. MODEL AND RESULTS

We construct the four-band tight-binding (TB) model by fitting the band structure to the *ab initio* results. The model parameters contain the NN hopping amplitude t , and NNN hopping t' and t'' with and without intermediating Cr atoms, respectively, as shown in Fig. 1(c). This model is similar to the common checkerboard lattice model except that there are four sites in one primitive cell. The extension of the primitive cell in $\text{CrCl}_2(\text{pyz})_2$ is due to the four different norm vector directions of pyrazine rings. The directed vector on the lattice sites leads to a nonsymmorphic space group because all rotational axes, including the out-of-plane fourfold rotation axis and the in-plane twofold rotation axis, pass through Cr atoms but the inversion centers are at the pyrazine ring centers. This nonsymmorphic property doubles the primitive cell compared to the checkerboard lattice and causes the degeneracy along the XM high-symmetry line. We construct the TB model respecting all symmetrical operations mentioned above. In addition, the four bands around the Fermi level are fully spin polarized in the spin-down channel. By ignoring SOC terms, the model can be constructed without considering the spin degree of freedom. Thus, this spinless model preserves the

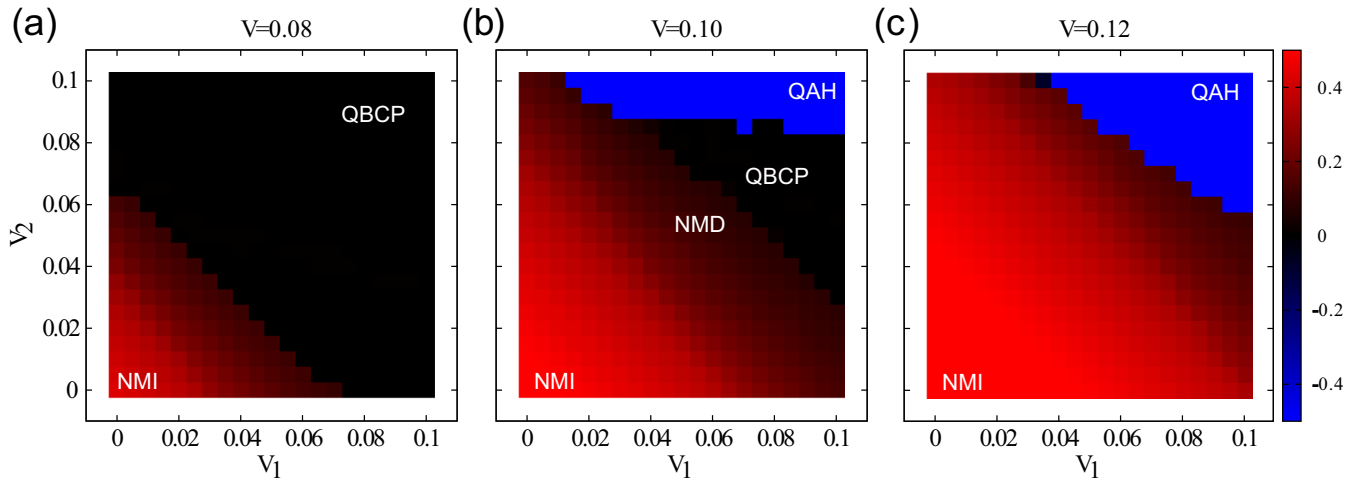


FIG. 2. (a)–(c) The mean-field phase diagram under different NN interaction V values. The order parameters of the nematic phase, including the site-nematic insulator (NMI) and site-nematic Dirac semimetal (NMD), are colored in red and the QAH order parameter is colored in blue. The ground states with negligible QAH and site-nematic order parameters are colored in black, where the QBCP at Γ persists.

time-reversal symmetry as manifested by the real number of hopping parameters. Compared to the two-site checkerboard lattice model, the QBCP on the M point now folds to Γ due to the doubling of the unit cell as shown in Fig. 1(c). As we know the QBCP is unstable against short-range interactions in the checkerboard lattice model, in the following we add the interaction terms in this doubled model to check which phase is the ground state under various interaction parameters when QBCP is gapped or split.

The interaction-driven phase transition on the two-site checkerboard lattice has been discussed in Refs. [18,19] and in those works only the NN repulsion V is investigated. Similarly, if only V is considered in this case, the realistic hopping parameters, namely $t'/t = -0.187$, $t''/t = -0.070$, will make the area of the V -driven QAH phase quite small and a tiny increase of temperature would kill it. Furthermore, the chemical potential does not pass the QBCP exactly, which weakens the instability of QBCP. To find a stable and relatively large portion of the QAH phase region, two types of NNN repulsion interactions are considered to compete with the NN repulsion (Fig. 1). Therefore, the total Hamiltonian reads as

$$\hat{H}_T = \hat{H}_{TB} + V \sum_{\langle ij \rangle} \hat{n}_i \hat{n}_j + V_1 \sum_{\langle\langle ij \rangle\rangle'} \hat{n}_i \hat{n}_j + V_2 \sum_{\langle\langle ij \rangle\rangle''} \hat{n}_i \hat{n}_j, \quad (1)$$

where \hat{n}_i is the density operator on site i , $\langle ij \rangle$ stands for the pair of NN sites, and $\langle\langle ij \rangle\rangle'$ ($\langle\langle ij \rangle\rangle''$) stands for the NNN site pair with (without) the Cr atom at the intersite. Details about the model can be found in the Supplemental Material [38].

This model was solved by using the Hartree-Fock variational method [39]. The mean-field Hamiltonian with variational parameters on every bond is used to provide the single-particle ground state. By searching the minimal point of total energy in the variational parameter space, one can get the ground state within the mean-field approximation level. Figures 2 and 3 show the phase diagram of the model within various interaction parameters. When the NNN repulsion interactions V_1 and V_2 are not applied, the observable phase transition occurs at $V = 0.053$ eV [Fig. 3(a)] from the normal

state to the site-nematic insulator (NMI) phase. The order parameter describing the nematic phase is defined as

$$\rho_{\text{NMI}} = \bar{n}_1 - \bar{n}_2, \quad (2)$$

where \bar{n}_i is the charge density on site i . At this phase, the charge redistribution on the four sites in one unit cell breaks

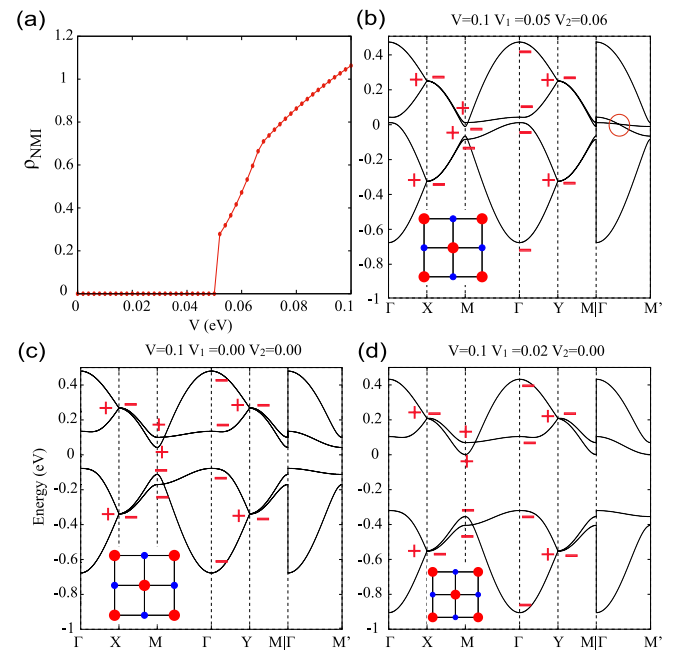


FIG. 3. (a) The order parameter of the NMI state evolves with V , and the other two interaction parameters are $V_1 = V_2 = 0$. The phase transition occurs at $V = 0.053$ eV from the normal state to the NMI phase. Fixing $V = 0.1$ eV, the dependence of the band structures on V_1 and V_2 is shown in (b) for the NMD state, and (c) and (d) for the NMI state. The insets are graphical plots of the corresponding ordered state in real space with the dot size representing the charge disproportion among the sites. The red circle in (b) marks the Dirac point. On each TRIM, the even and odd parities of the occupied bands are labeled with + and -, respectively.

the fourfold rotation into a twofold one. Two sites connected by one of the diagonal lines accommodate more electrons than the other two, as schematically shown in the inset of Fig. 3. The energy gap in that phase is quite large and the occupied states do not hold a nontrivial topological property as can be seen from the parities of the occupied state in Fig. 3(c). This topological trivial phase can be well understood by the EBR analysis. Without fourfold rotation, the two sites with more electron accumulation can form a complete EBR in the new phase, which is topologically equivalent to an atomic insulator. Note that the QAH phase is hard to be observed in this model with only NN repulsion because t'/t is fairly small as shown in Fig. 2(a), which is consistent with previous results [18,19].

Introducing the NNN repulsion leads to the competition between NMI and other states. As we can see from Fig. 2, with a relatively small V value, the growing of V_1 and V_2 recovers the normal state with QBCP within the mean-field calculation. This is easy to understand because the increase of charge on the two diagonal atoms would save energy when only NN repulsion is applied. But as the NNN repulsion increases, it would cost more energy to maintain an imbalanced charge distribution. When introducing the NNN repulsion, the NMI still exists in the area where the NNN repulsion is weak. We also find a nematic Dirac semimetal (NMD) state as a transition state between the NMI and normal state as shown in Fig. 2(b). In that phase, the redistribution of charge tends to cause a band inversion at the M point to recover an atomic insulator and the splitting of QBCP into two Dirac points along $\Gamma M'$ [Fig. 3(b)]. As the parameters are approaching the NMI phase, the Dirac points move towards the M' point. Finally they merge at M' or M and open a gap. The band inversion happens at the same time and makes the NMI phase trivial. Notice that the NMD state has not been found in the two-site checkerboard lattice model because the interaction strength and hopping amplitude need fine tuning.

Interestingly, for some proper V values, the time-reversal symmetry breaking QAH phase would appear spontaneously in a considerably large parameter space. The order parameter describing the QAH phase is defined as

$$\rho_{\text{QAH}} = \text{Im} \sum_{\langle ij \rangle} \sum_{n,k} (\langle p_i | \psi_{n,k} \rangle \langle \psi_{n,k} | p_j \rangle), \quad (3)$$

where $|p_i\rangle$ means the local orbital on site i in the home cell and $|\psi_{n,k}\rangle$ is the eigenfunction of the n th band at k . $\langle ij \rangle$ runs over the NN bond pair of $\langle 12 \rangle$, $\langle 24 \rangle$, $\langle 43 \rangle$, $\langle 31 \rangle$. n is the occupied band and k samples the whole BZ. The nonzero order parameter indicates the existence of the imaginary part of NN hopping, which causes a staggered chiral flux pattern and breaks time-reversal symmetry. The flux configuration is shown in Fig. 3(a) with its band structure. In the QAH phase, all in-plane C_2 symmetries are broken but C_4 and inversion are preserved. This set of symmetry operations do not protect any twofold degeneracy at Γ and the system becomes gapped. Due to the C_4 symmetry, charges still distribute equally on the four sites, and the two occupied bands cannot form a complete EBR. The occupied states must possess nontrivial topological properties. As show in Fig. 3(a), we label the parity on every TRIM point for the bands. The parity of the Chern number

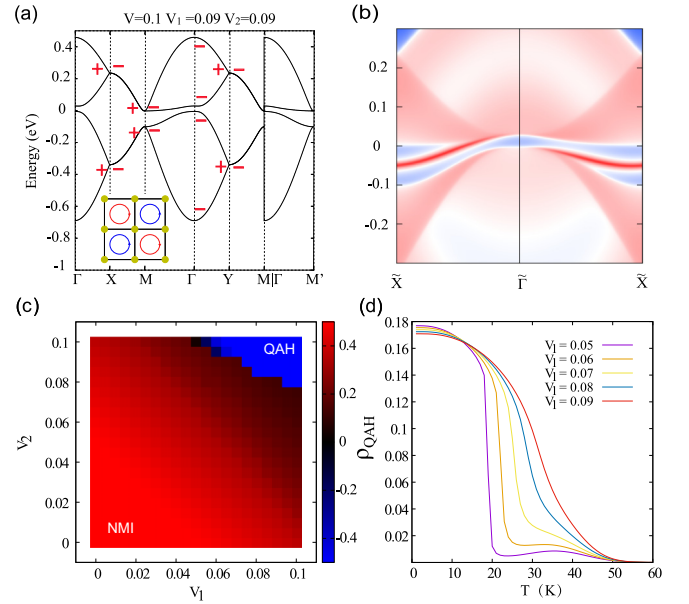


FIG. 4. (a) The band structures of the QAH phase, where the charge is distributed equally, but there exists an imaginary part of hopping on the nearest bonds, which forms a staggered flux pattern as shown in the inner window. (b) The chiral edge state of the QAH state in (a). (c) The phase diagram of the C_4 breaking model with $m = 0.0025$. (d) The order parameter of the QAH state evolves with temperature. The other two interaction parameters are $V = 0.1$, $V_2 = 0.09$.

can be calculated by using the following formula [40],

$$(-1)^{\text{Chern}} = \prod_{\mathbf{K}_{\text{TRIM}}} \xi(\mathbf{K}_{\text{TRIM}}), \quad (4)$$

where $\xi(\mathbf{K}_{\text{TRIM}}) = \prod_n \xi_n(\mathbf{K}_{\text{TRIM}})$ and $\xi_n(\mathbf{K}_{\text{TRIM}})$ is the parity of the n th occupied Bloch state at the TRIM point \mathbf{K}_{TRIM} . The chiral edge state [41] of the QAH phase is shown in Fig. 3(b).

To illustrate the stability of this interaction-induced QAH state, we further investigate the perturbations of breaking C_4 symmetry and increasing temperature. We find that although the QBCP is protected by the C_4 symmetry, the QAH phase can still emerge under proper interaction parameters when C_4 breaking terms are added to the model. Figure 4(c) shows the phase diagram when including the following perturbation term,

$$\delta H(k) = m\sigma_z \otimes \sigma_z, \quad (5)$$

which is k independent as long as the perturbation is an on-site term. Therefore, the ground state only preserves the inversion symmetry because the QAH order and nematic charge distribution appear simultaneously. In Fig. 4(d), it is shown that the QAH phase is suppressed by increasing temperature. The model with a larger interaction strength will lead to a more stable QAH ground state against the temperature, which is consistent with previous studies [18,19].

In Table I, we summarized the preserved and broken symmetries of all the phases mentioned above. There exist other types of phases such as stripe charge order when V_1 or V_2 are set to be much larger than V . But under a reasonable assumption that the interaction with the shorter distance

TABLE I. Symmetry properties for the various ordered states.

	I	$\tilde{C}_{4,001}$	$C_{2,110}$	$\tilde{C}_{2,010}$
QBCP	✓	✓	✓	✓
QAH	✓	✓	✗	✗
NMI	✓	✗	✓	✗
NMD	✓	✗	✓	✗

would have the larger strength, we do not discuss these cases in this paper.

IV. CONCLUSION

In summary, first-principles calculations of ferromagnetic van der Waals layered metal-organic framework $\text{CrCl}_2(\text{pyz})_2$ exhibit a quadratic band crossing at the Γ point when C_4 is preserved. To describe the low-energy bands, we established a C_4 symmetric TB model by using the effective p -type molecular orbitals sitting on the center of each pyrazine ring. Due to the insulating ground state indicated by the experiments, we added the short-ranged repulsive interactions on the TB

model. There are fruitful ordered phases to be the ground state as we tune the interaction parameters, including the QAH, NMI, and NMD states. The QAH state is prominent by the spontaneous appearance of time-reversal breaking staggered chiral flux. The QAH phase is stable against the C_4 breaking perturbation in the TB model. These ordered phases may appear in this family of metal-organic frameworks with different transition-metal elements or bond lengths, which can tune several items including the interaction strength or hopping amplitude.

ACKNOWLEDGMENTS

This work was supported by the National Natural Science Foundation of China (Grants No. 11974395, No. 11925408, No. 11921004, and No. 12188101), the Ministry of Science and Technology of China (Grants No. 2018YFA0305700 and No. 2022YFA1403800), the Chinese Academy of Sciences (Grant No. XDB33000000) and the Informatization Plan of the Chinese Academy of Sciences (Grant No. CAS-WX2021SF-0102), the Hong Kong Research Grants Council (Projects No. GRF16300918 and No. 16309020), and the Center for Materials Genome.

-
- [1] F. D. M. Haldane, *Phys. Rev. Lett.* **61**, 2015 (1988).
- [2] X.-L. Qi, Y.-S. Wu, and S.-C. Zhang, *Phys. Rev. B* **74**, 085308 (2006).
- [3] R. Yu, W. Zhang, H.-J. Zhang, S.-C. Zhang, X. Dai, and Z. Fang, *Science* **329**, 61 (2010).
- [4] G. Xu, H. Weng, Z. Wang, X. Dai, and Z. Fang, *Phys. Rev. Lett.* **107**, 186806 (2011).
- [5] K.-Y. Yang, Y.-M. Lu, and Y. Ran, *Phys. Rev. B* **84**, 075129 (2011).
- [6] Z. Qiao, X. Li, W.-K. Tse, H. Jiang, Y. Yao, and Q. Niu, *Phys. Rev. B* **87**, 125405 (2013).
- [7] C.-Z. Chang, J. Zhang, X. Feng, J. Shen, Z. Zhang, M. Guo, K. Li, Y. Ou, P. Wei, L.-L. Wang, Z.-Q. Ji, Y. Feng, S. Ji, X. Chen, J. Jia, X. Dai, Z. Fang, S.-C. Zhang, K. He, Y. Wang *et al.*, *Science* **340**, 167 (2013).
- [8] H. Weng, R. Yu, X. Hu, X. Dai, and Z. Fang, *Adv. Phys.* **64**, 227 (2015).
- [9] J. G. Checkelsky, R. Yoshimi, A. Tsukazaki, K. S. Takahashi, Y. Kozuka, J. Falson, M. Kawasaki, and Y. Tokura, *Nat. Phys.* **10**, 731 (2014).
- [10] Y. Gong, J. Guo, J. Li, K. Zhu, M. Liao, X. Liu, Q. Zhang, L. Gu, L. Tang, X. Feng, D. Zhang, W. Li, C. Song, L. Wang, P. Yu, X. Chen, Y. Wang, H. Yao, W. Duan, Y. Xu *et al.*, *Chin. Phys. Lett.* **36**, 076801 (2019).
- [11] J. Li, Y. Li, S. Du, Z. Wang, B.-L. Gu, S.-C. Zhang, K. He, W. Duan, and Y. Xu, *Sci. Adv.* **5**, eaaw5685 (2019).
- [12] Y. Deng, Y. Yu, M. Z. Shi, Z. Guo, Z. Xu, J. Wang, X. H. Chen, and Y. Zhang, *Science* **367**, 895 (2020).
- [13] S. Raghu, X.-L. Qi, C. Honerkamp, and S.-C. Zhang, *Phys. Rev. Lett.* **100**, 156401 (2008).
- [14] W. Zhu, S.-S. Gong, T.-S. Zeng, L. Fu, and D. N. Sheng, *Phys. Rev. Lett.* **117**, 096402 (2016).
- [15] Y. Wang, Z. Wang, Z. Fang, and X. Dai, *Phys. Rev. B* **91**, 125139 (2015).
- [16] K. Sun and E. Fradkin, *Phys. Rev. B* **78**, 245122 (2008).
- [17] X. Feng, K. Jiang, Z. Wang, and J. Hu, *Sci. Bull.* **66**, 1384 (2021).
- [18] K. Sun, H. Yao, E. Fradkin, and S. A. Kivelson, *Phys. Rev. Lett.* **103**, 046811 (2009).
- [19] H.-Q. Wu, Y.-Y. He, C. Fang, Z. Y. Meng, and Z.-Y. Lu, *Phys. Rev. Lett.* **117**, 066403 (2016).
- [20] J. M. Murray and O. Vafek, *Phys. Rev. B* **89**, 201110(R) (2014).
- [21] S. Sur, S.-S. Gong, K. Yang, and O. Vafek, *Phys. Rev. B* **98**, 125144 (2018).
- [22] Q.-F. Liang, J. Zhou, R. Yu, X. Wang, and H. Weng, *Phys. Rev. B* **96**, 205412 (2017).
- [23] W.-F. Tsai, C. Fang, H. Yao, and J. Hu, *New J. Phys.* **17**, 055016 (2015).
- [24] D. Wu, Y. Huang, S. Sun, J. Gao, Z. Guo, H. Weng, Z. Fang, K. Jiang, and Z. Wang, *Sci. China Phys. Mech. Astron.* **65**, 256811 (2022).
- [25] K. S. Pedersen, P. Perlepe, M. L. Aubrey, D. N. Woodruff, S. E. Reyes-Lillo, A. Reinholdt, L. Voigt, Z. Li, K. Borup, M. Rouzières *et al.*, *Nat. Chem.* **10**, 1056 (2018).
- [26] W. Hu, K. Yang, A. Stroppa, A. Continenza, and H. Wu, *J. Mater. Chem. C* **9**, 5985 (2021).
- [27] H. Xie, Y. Qie, I. Muhammad, and Q. Sun, *J. Phys.: Condens. Matter* **32**, 135801 (2020).
- [28] P. Perlepe, I. Oyarzabal, A. Mailman, M. Yquel, M. Platonov, I. Dovgaliuk, M. Rouzières, P. Negrier, D. Mondieig, E. A. Sutura, M.-A. Dourges, S. Bonhommeau, R. A. Musgrave, K. S. Pedersen, D. Chernyshov, F. Wilhelm, A. Rogalev, C. Mathoniere, and R. Clerac, *Science* **370**, 587 (2020).

- [29] W. Kohn and L. J. Sham, *Phys. Rev.* **140**, A1133 (1965).
- [30] G. Kresse and J. Furthmüller, *Phys. Rev. B* **54**, 11169 (1996).
- [31] J. P. Perdew, K. Burke, and M. Ernzerhof, *Phys. Rev. Lett.* **77**, 3865 (1996).
- [32] J. P. Perdew, K. Burke, and M. Ernzerhof, *Phys. Rev. Lett.* **78**, 1396(E) (1997).
- [33] H. J. Monkhorst and J. D. Pack, *Phys. Rev. B* **13**, 5188 (1976).
- [34] S. L. Dudarev, G. A. Botton, S. Y. Savrasov, C. J. Humphreys, and A. P. Sutton, *Phys. Rev. B* **57**, 1505 (1998).
- [35] B. Bradlyn, L. Elcoro, J. Cano, M. G. Vergniory, Z. Wang, C. Felser, M. I. Aroyo, and B. A. Bernevig, *Nature (London)* **547**, 298 (2017).
- [36] J. Cano, B. Bradlyn, Z. Wang, L. Elcoro, M. G. Vergniory, C. Felser, M. I. Aroyo, and B. A. Bernevig, *Phys. Rev. B* **97**, 035139 (2018).
- [37] J. Gao, Q. Wu, C. Persson, and Z. Wang, *Comput. Phys. Commun.* **261**, 107760 (2021).
- [38] See Supplemental Material at <http://link.aps.org/supplemental/10.1103/PhysRevB.106.235103> for details of the TB model and the Hartree-Fock method.
- [39] J. Liu and X. Dai, *Phys. Rev. B* **103**, 035427 (2021).
- [40] Y. J. Jin, R. Wang, B. W. Xia, B. B. Zheng, and H. Xu, *Phys. Rev. B* **98**, 081101(R) (2018).
- [41] Q. Wu, S. Zhang, H.-F. Song, M. Troyer, and A. A. Soluyanov, *Comput. Phys. Commun.* **224**, 405 (2018).